Thymosin β_4 Induces a Conformational Change in Actin Monomers

Irina V. Dedova,* Olga P. Nikolaeva,† Daniel Safer,‡ Enrique M. De La Cruz,§ and Cris G. dos Remedios*
*Muscle Research Unit, Institute for Biomedical Research, University of Sydney, New South Wales, Australia; †Belozersky Institute of Physico-Chemical Biology, Lomonosov Moscow State University, Moscow, Russia; ‡Pennsylvania Muscle Institute and Department of Physiology, University of Pennsylvania, School of Medicine, Philadelphia, Pennsylvania; and §Department of Molecular Biophysics and Biochemistry, Yale University, New Haven, Connecticut

ABSTRACT Using fluorescence resonance energy transfer spectroscopy we demonstrate that thymosin β_4 ($t\beta_4$) binding induces spatial rearrangements within the small domain (subdomains 1 and 2) of actin monomers in solution. $T\beta_4$ binding increases the distance between probes attached to Gln-41 and Cys-374 of actin by 2 Å and decreases the distance between the purine base of bound ATP (εATP) and Lys-61 by 1.9 Å, whereas the distance between Cys-374 and Lys-61 is minimally affected. Distance determinations are consistent with $t\beta_4$ binding being coupled to a rotation of subdomain 2. By differential scanning calorimetry, $t\beta_4$ binding increases the cooperativity of ATP-actin monomer denaturation, consistent with conformational rearrangements in the $t\beta_4$-actin complex. Changes in fluorescence resonance energy transfer are accompanied by marked reduction in solvent accessibility of the probe at Gln-41, suggesting it forms part of the binding interface. $T\beta_4$ and cofilin compete for actin binding. $T\beta_4$ concentrations that dissociate cofilin from actin do not dissociate the cofilin-DNase I-actin ternary complex, consistent with the DNase binding loop contributing to high-affinity $t\beta_4$-binding. Our results favor a model where thymosin binding changes the average orientation of actin subdomain 2. The $t\beta_4$-induced conformational change presumably accounts for the reduced rate of amide hydrogen exchange from actin monomers and may contribute to nucleotide-dependent, high affinity binding.

INTRODUCTION

The actin cytoskeleton plays a central role in the basic functions of eukaryotic cells such as maintenance of cell shape, cytoplasmic organization, cell movement, and cell division. This is achieved through a dynamic equilibrium between polymeric and monomeric actin. Many actin-binding proteins (ABP) that regulate the monomer-to-polymer transition by binding monomers, filaments or both, have been identified (1). Thymosin β_4 ($t\beta_4$) is a small ($M_r < 5$ kDa) member of a highly conserved family of actin monomer-sequestering proteins present in actively motile cells, developing chick brain, and embryonic skeletal muscle (1,2). $T\beta_4$ forms a 1:1 complex with monomeric actin and can bind to F-actin at high concentrations (3,4). β-thymosins are the principal in vivo regulators of unpolymerized actin, and are essential for maintaining the cytoplasmic pool of actin monomers required for rapid filament elongation (reviewed in (1)).

The exact $t\beta_4$ binding surfaces on the actin monomer are unknown and several models have been proposed (4–7). There is a general agreement that subdomains 1 and 3 (SD1 and SD3) of actin form part of the interface, similar to gelsolin and profilin, accounting for competitive binding (8,9). Binding to SD1 and SD3 is expected to restrict propeller-type opening and closing motion of the two major domains (10). However, there is disagreement over the role of SD2 of actin in binding $t\beta_4$. It has been proposed that the C-terminal region of $t\beta_4$ binds directly to the DNase I-binding loop (5) because it can be chemically crosslinked to residues of the DNase I-binding loop in SD2 (5,8). The nucleotide-dependence of SD2 conformation (11) could therefore account for the nucleotide-dependence of $t\beta_4$ binding affinity (12). Subtilisin cleavage of actin in the DNase I-binding loop causes a twofold decrease in the affinity of $t\beta_4$ (13), consistent with SD2 contributing to the stability and strength of the actin-$t\beta_4$ interaction. Image reconstruction of actin filaments chemically crosslinked to $t\beta_4$ (4) suggests $t\beta_4$ binds SD2 and SD4 as well as the gap between SD1 and SD2 (5). Binding of $t\beta_4$ to actin monomers is coupled to a change in heat capacity, dissociation of bound waters, a reduction in amide hydrogen exchange (5), and inhibition of nucleotide exchange (3). It was hypothesized that $t\beta_4$ folding upon binding could account for the change in heat capacity (5), and recent evidence favors this interpretation (13). It was also proposed that $t\beta_4$ binding inhibits the movement and separation of SD2 and SD4, closing the nucleotide-binding cleft and reducing the rates of nucleotide and amide hydrogen exchange (5). In this report, we used fluorescence spectroscopy to test the hypothesis that $t\beta_4$ changes the actin monomer conformation (5) and evaluate the contributions of actin SD2 to $t\beta_4$ binding. Our results are consistent with $t\beta_4$ binding to SD1, SD2 and SD3, causing changes in the spatial orientation of actin monomer subdomains.

Submitted March 16, 2005, and accepted for publication October 17, 2005.

Address reprint requests to Enrique M. De La Cruz, Yale University, Dept. of Molecular Biophysics and Biochemistry, PO Box 208114, New Haven, CT 06520-8114. Tel.: 203-432-5424; Fax 203-432-1296; E-mail: enrique.delacruz@yale.edu.

0006-3495/06/02/985/08 $2.00

MATERIALS AND METHODS

5-(((2-Iodoacetyl)amino)ethyl)aminonaphthalene-1-sulfonic acid (IAEDANS), 1,N^6-ethenoadenosine-5′-triphosphate (εATP), dansyl cadaverine (DC), and fluorescein-5-isothiocyanate (FITC) were purchased from Molecular Probes

doi: 10.1529/biophysj.105.063081

(Eugene, OR). *N*-(4-(dimethylamino)-3,5-dinitrophenyl)-maleimide (DDPM) and *N*-ethylmaleimide (NEM) were from Sigma-Aldrich (St. Louis, MO). Rabbit skeletal muscle actin was prepared in G buffer (5 mM imidazole, pH 7.0, 0.2 mM ATP, 0.1 mM $CaCl_2$, 0.5 mM DTT, and 1 mM NaN_3). $T\beta_4$ was isolated from bovine spleen (8). Bovine pancreatic DNase I (DPRF grade) was from Worthington Biochemicals (Lakewood, NJ). Cofilin was prepared as a recombinant protein using a cDNA sequence derived from chick embryo, kindly supplied by Dr. Takashi Obinata (Chiba, Japan). Concentrations of actin, DNase I, and cofilin were determined using extinction coefficients of 0.63 cm^{-1} (0.1%, 290 nm), 1.1 cm^{-1} (0.1%, 280 nm), and 0.98 cm^{-1} (0.1%, 280 nm), respectively. Actin was labeled with the following fluorescent probes as described: *a*), DC (14); *b*), DC-actin further modified with DDPM (14); *c*), IAEDANS (15); *d*), NEM or FITC (16); and *e*), ε-ATP (17). The following molar extinction coefficients were used for probes bound to actin: DC, 4640 M^{-1} cm^{-1} at 330 nm and DDPM, 3050 M^{-1} cm^{-1} at 440 nm (14); IAEDANS, 6100 M^{-1} cm^{-1} at 336 nm (15); and FITC, 74,500 M^{-1} cm^{-1} at 493 nm (18). The concentration of actin in labeled samples was determined by the DC Protein Assay ($\lambda = 795$ nm, Bio-Rad Laboratories, Hercules, CA) using unlabeled actin as the standard. The typical labeling ratios were: 0.63–0.9 for DC ($n = 10$); 0.5–0.85 for DDPM ($n = 7$); 0.8–0.98 for IAEDANS ($n = 10$); and 0.85–1.0 for FITC ($n = 9$). Bound ATP was exchanged with εATP as described earlier (17). In brief, nonlabeled or FITC-labeled G-actin (24–48 μM) was treated with 0.1 volumes of Dowex-1 on ice for 10 min to remove free ATP. Dowex-1 was removed by filtration and the solution was supplemented with 0.5 mM εATP, 0.1 mM $CaCl_2$, and 1 mM Tris/HCl (pH 8.0) and equilibrated on ice overnight. This procedure was repeated again to ensure a complete exchange of bound ATP with εATP. Free nucleotide was removed with Dowex-1 immediately before fluorescence experiments. Because the actin concentrations used are much higher than the K_d for nucleotide binding (19), bound nucleotide will not dissociate to any appreciable extent during the time-course of the experiments.

Fluorescence measurements were carried out in G buffer at 10°C in a temperature-controlled cuvette using an SLM 48000 S Multiple Frequency Lifetime Spectrofluorometer (SLM Aminco, Foster City, CA) operating on a xenon arc lamp essentially as described (14). All experiments were repeated 5–10 times and results were presented as means ± SE. Fluorescence resonance energy transfer (FRET) efficiency (E) was determined from the intensities of the donor (D) in the presence (F_{DA}) and absence (F_D) of the acceptor (A) according to Eq. 1: $E = (1 - F_{DA}/F_D)/\alpha$, where α is a degree of labeling with the acceptor in the double-labeled actin. Intensities were normalized to the D-concentration after background subtraction. Energy transfer efficiency is related to distance separating D- and A-probes according to Eq. 2: $E = R_o^6/(R_o^6+R^6)$. R_o is the Förster critical distance between the D and A (when $E = 0.5$) defined by Eq. 3: $R_o^6 = (8.79 \times 10^{-11})n^{-4}\kappa^2 Q_D J$, where n is the refractive index of the medium, κ^2 is the orientation factor, Q_D is the quantum yield of the D on actin in the absence of the A, and J is the overlap integral given in M^{-1} cm^{-1} nm^4. R_o distances of actin alone were taken as 49.6 Å for IAEDANS/FITC (20) and 47.4 Å for εATP/FITC (17). These values were corrected for changes in the donor quantum yield (21) due to $t\beta_4$ binding. The R_o for DC/DDPM was obtained experimentally using fluorescence emission spectrum of the DC-actin in the presence of nonfluorescent DDPM and the absorption spectrum of the DDPM-actin, taking $\kappa^2 = 2/3$. FRET measurements between the following positions were done using the following donor-acceptor pairs as described: *a*), DC (Gln-41) and DDPM (Cys-374) (14); *b*), IAEDANS (Cys-374) and FITC (Lys-61) (17); and *c*), εATP (nucleotide-binding cleft) and FITC (Lys-61) (17). Intensities of the probe in the D-only and D/A samples were normalized to the fluorophore concentration by overnight tryptic digestion, as described (17). In brief, 0.2–0.4 mg ml^{-1} of trypsin in G-buffer was added into the D and D/A sample solutions after FRET measurements. After digestion, the amino-acid residues with D- and A-probes were separated, abolishing FRET. Thus, fluorescence intensities were directly proportional to the concentration of the D-probe in solution. The ratio of these fluorescence intensities was taken to be proportional to $F_{DA} \times C_i/F_D \times C_i'$ (Eq. 4), where C_i and C_i' are the concentrations of D in D and D/A samples, respectively. Acrylamide quenching of DC-actin fluorescence ($\lambda_{ex} = 332$ nm, $\lambda_{em} = 512$ nm) was performed at 22°C in a thermostated cuvette as described (14). The apparent Stern-Volmer constant (K_{SV}) was obtained from the slope of a plot of F_o/F versus [acrylamide] by fitting to Eq. 5 as $F_o/F = 1 + K_{SV}$ [Q], where Q is the quencher, i.e., acrylamide.

SDS PAGE and native 10% PAGE gels were done following standard protocols (22). After FRET measurements, labeled actin and its complexes were mixed with equal volumes of native sample buffer (62.5 mM Tris-Cl, pH 6.8, 10% glycerol, and 0.1% bromophenol blue) and separated by native PAGE gel electrophoresis at 70–110 V for 90–120 min in an ice bath (23). Differential scanning calorimetry (DSC) was performed on a DASM-4M differential scanning microcalorimeter (Institute for Biological Instrumentation, Pushchino, Russia) as described (24). The scanning rate was 1 K min^{-1}. Transition temperatures (T_m) were determined from the peak of thermal transition, and the apparent enthalpies (ΔH°_{app}) were calculated from the integrated areas of the denaturation peaks.

RESULTS

Effect of $t\beta_4$ on the distance between Gln-41 and Cys-374 of actin

A donor probe, DC, at Gln-41 and an acceptor, DDPM, at Cys-374 (Fig. 1), located on opposite sides of the small domain of actin were used to measure FRET along the SD1 and SD2 axis. Fig. 2 *A* shows corrected and averaged ($n = 5$) fluorescence emission spectra of DC-actin (*curve 1*) and DDPM-DC-actin (*curve 2*). A calculated value of 30.3 Å for R_0 of the DC/DDPM pair in actin alone ($J = 9.8 \times 10^{15}$ M^{-1} cm^{-1} nm^4) and a FRET efficiency of 0.268 ± 0.03 correspond to a distance of 35.8 ± 1.0 Å between these probes. Note that the emission maximum of DC is shifted by 15 nm to the longer wavelength in the presence of DDPM, suggestive of a possible allosteric effect caused by a modification of Cys-374 consistent with reports on the allosteric relationship between SD1 and SD2 (25).

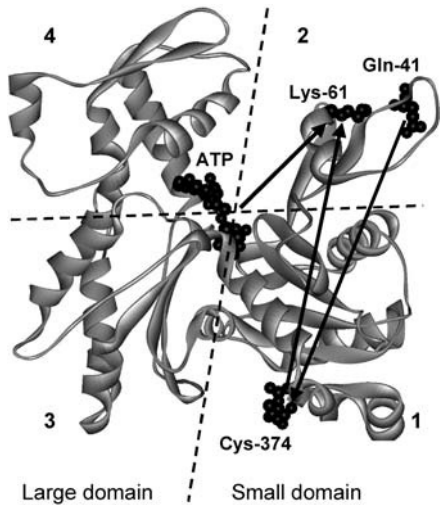

FIGURE 1 Position of the donor/acceptor probe pairs used for FRET measurements in actin. Gln-41, Lys-61, Cys-374, and ATP are shown as space-filled structures (26). The numerals refer to the four subdomains.

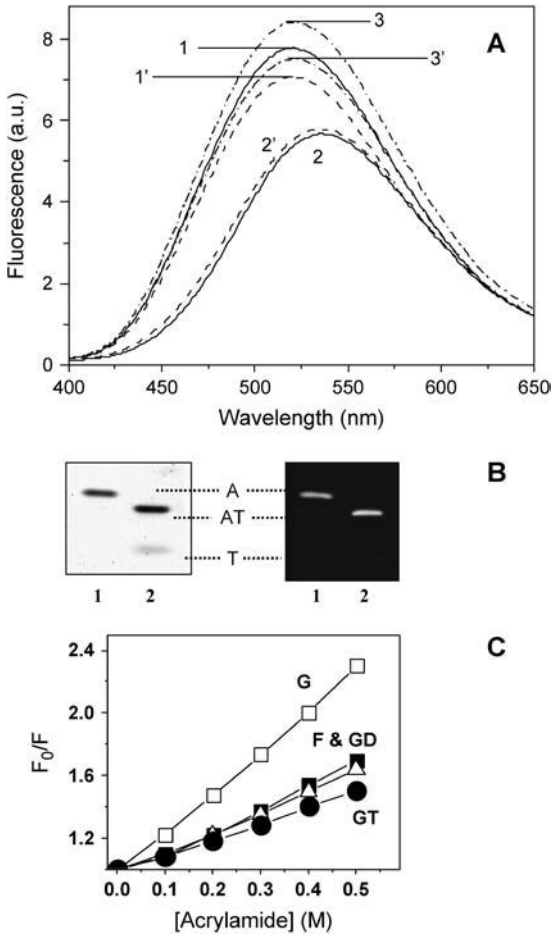

FIGURE 2 Effect of $t\beta_4$ on the distance between Gln-41 and Cys-374 of actin. Corrected and averaged fluorescence spectra ($\lambda_{ex} = 332$ nm and $\lambda_{em} = 525$ nm) of DC- and DC/DDPM-actin in the presence and absence of $t\beta_4$. (*A*) DC- and DC/DDPM-actin (2–5 μM) before (*solid curves 1* and *2*, respectively) and after addition of a 10-fold molar excess of $t\beta_4$ (*dashed curves 1′* and *2′*, respectively); and DC/NEM-actin in the presence and absence of $t\beta_4$ (*dash-dot curves 3* and *3′*, respectively). (*B*) (*Left*) A Coomassie-stained 12% native PAGE gel of DC/DDPM-actin (*lane 1*) and its binary complex with $t\beta_4$ (*lane 2*). (*Right*) The same gel viewed under UV light. (Symbols: *A*, monomeric actin; *T*, $t\beta_4$; and *AT*, actin/$t\beta_4$ complex.) (*C*) Stern-Volmer quenching plots: open squares, DC-actin monomers; solid squares, DC-actin filaments; circles, the actin monomer/$t\beta_4$ complex; and triangles, the DNase I/actin monomer complex. All samples were in G-buffer except DC-actin filaments that additionally contained 50 mM KCl and 2 mM $MgCl_2$. The temperature was constant (22°C).

Bound $t\beta_4$ decreases the intensity of DC-actin by 12 ± 2% (*dashed* curve *1′*, $n = 5$) in agreement with a previous report (8). However, in the presence of DDPM this decrease is abolished (*dashed curve 2′*). The resulting FRET efficiency calculated using $R_0 = 29.4$ Å (corrected for changes in the Q_D) is 0.182 ± 0.03, which corresponds to a distance of 37.8 ± 1.2 Å between DC and DDPM in the actin-$t\beta_4$ complex. Thus, $t\beta_4$ increases the distance between the probes attached to Cys-374 and Gln-41 by 2 Å ($p < 0.000$). Since DDPM modification of Cys-374 induces an allosteric effect on the actin monomer conformation, we modified DC-actin with NEM at Cys-374, and repeated the FRET experiments using DC/NEM-actin as a donor-only sample. The NEM probe has no absorbance in the overlap region of the donor emission, and therefore, there is no FRET between these two probes. Fluorescence intensity of DC slightly increases in the presence of NEM (*dash-dot curve 3*, $n = 5$). However, it has no significant effect on the final distance. Using $R_0 = 31.05$ Å (recalculated for changes in the Q_D of DC in the presence of NEM), and the efficiency of 0.307 ± 0.03 ($n = 5$), the calculated distance between the probes attached to Gln-41 and Cys-374 is 35.5 ± 0.9 Å. The addition of $t\beta_4$ to DC/NEM-actin (*dash-dot curve 3′*) results in a decrease in fluorescence intensity by 13 ± 4%, i.e., similar to NEM-unmodified DC-actin. The calculated efficiency of 0.191 ± 0.02 ($n = 5$) yields a distance of 37.4 ± 1.0 Å between DC and DDPM in the presence of $t\beta_4$. Thus, $t\beta_4$ increases the measured distance by ~2 Å. Native PAGE gels (Fig. 2 *B*) demonstrate that concentrations of $t\beta_4$ used in FRET experiments are sufficient to saturate labeled actin as expected from the equilibrium binding affinities (5). The $t\beta_4$-induced increase in the Gln-41/Cys-374 distance is accompanied by a reduction in the solvent accessibility of Gln-41 (Fig. 2 *C*). Acrylamide quenches the fluorescence emission of DC in the G-actin/$t\beta_4$ complex (*curve GT*, $K_{SV} = 1.0 \pm 0.3$, $n = 6$) less efficiently than in G-actin alone (*curve G*, $K_{SV} = 2.4 \pm 0.1$, $n = 6$). A similar effect is observed in F-actin (*curve F*, $K_{SV} = 1.3 \pm 0.1$, $n = 5$) and in the actin-DNase I complex (*curve GD*, $K_{SV} = 1.2 \pm 0.1$, $n = 6$) where Gln-41 is protected from solvent because it forms part of the binding interface (26).

Effect of $t\beta_4$ on the distance between Lys-61 and Cys-374 of actin

Actin labeled with an IAEDANS (donor) at Cys-374 and a FITC (acceptor) at Lys-61 (Fig. 1) has a FRET efficiency of 0.65 ± 0.04 corresponding to a distance of 44.7 ± 1.1 Å, in agreement with a previous report (20). The fluorescence emission spectrum of IAEDANS-actin (Fig. 3 *A*, *solid curve 1*) demonstrates that $t\beta_4$ binding (*dashed curve 1′*) generates a 39 ± 3% ($n = 10$) decrease in fluorescence intensity at 475 nm and an 11-nm red shift of the emission maximum wavelength (5). However, in the presence of FITC (*solid curve 2*), $t\beta_4$ causes only a 27 ± 4% decrease ($\lambda = 475$ nm, $n = 9$) of the D-fluorescence intensity (*dashed curve 2′*). The difference demonstrates that there is a reduction in FRET efficiency between the probes at Cys-374 and Lys-61 when $t\beta_4$ is bound. The ratios of corrected fluorescence intensities (F_{DA} to F_D at $\lambda = 475$ nm) of the IAEDANS-actin/$t\beta_4$ (*dashed curve 1′*) and IAEDANS/FITC-actin/$t\beta_4$ complexes (*dashed curve 2′*) yields a FRET efficiency of 0.59 ± 0.04 ($n = 9$). Q_D of the D significantly decreases in the presence of $t\beta_4$ (0.48 in actin alone compared to ~0.3 in the actin/$t\beta_4$ complex, $n = 6$). This reduces R_0 from 49.6 Å (in actin alone) to 46.5 Å (in the actin/$t\beta_4$ complex), yielding a distance between IAEDANS and FITC in the actin/$t\beta_4$

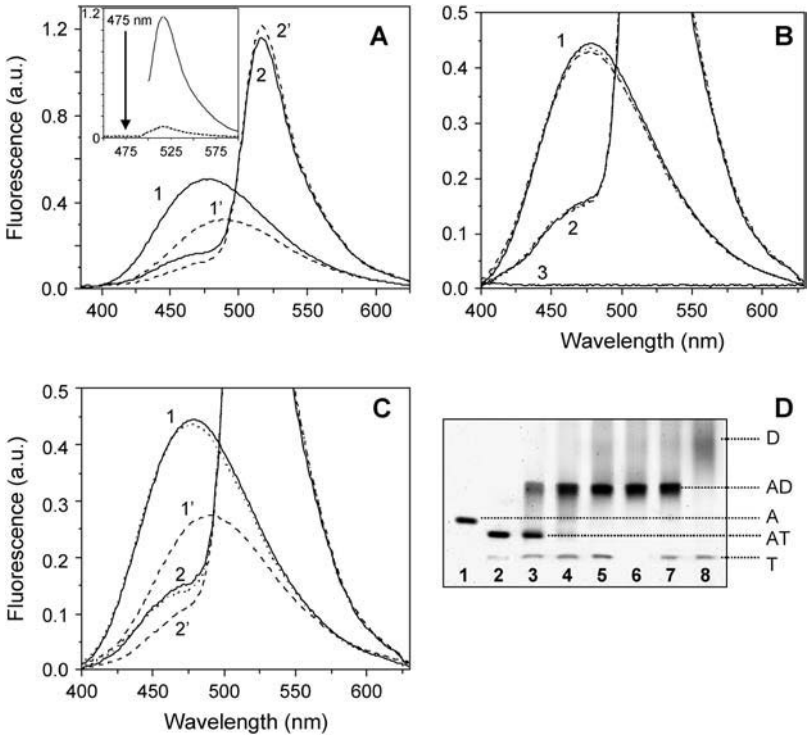

FIGURE 3 Effect of $t\beta_4$ on the distance between Lys-61 and Cys-374 of actin. (*A*) Corrected and averaged fluorescence spectra (λ_{ex} = 365 nm and λ_{em} = 520 nm) of IAEDANS-actin and IAEDANS/FITC-actin (1.5–3 μM) in the presence (*dashed curves 1′* and *2′*) and absence (*solid curves 1* and *2*) of 10-fold molar excess of $t\beta_4$. Conditions: G-buffer, 22°C. Spectra were normalized to a 100% acceptor labeling ratio. (*Inset*) The emission spectrum of FITC-actin excited at 520 nm (*solid curve*) and at 360 nm (*dashed curve*). (*B*) Effect of DNase I on the corrected and averaged fluorescence spectra of IAEDANS- and IAEDANS/FITC-actin (1.5–3 μM; *solid curves 1* and *2*, respectively) in the presence (*dashed curves 1* and *2*) and absence (*dotted curves 1* and *2*) of a 10-fold molar excess of $t\beta_4$. Curve *3* shows an emission spectrum of G-buffer. (*C*) The reverse order of ABP addition, i.e., $t\beta_4$ (*dashed curves*) followed by the DNase I (*dotted curves*). (*D*) A 10% Native PAGE gel. (*Lane 1*) IAEDANS/FITC-actin (3 μM) alone; (*lane 2*) 3 μM actin + 20 μM $t\beta_4$; (*lanes 3–5*) 1.5, 3, and 6 μM DNase I was added to the actin/$t\beta_4$ complex; (*lane 6*) 3 μM actin + 6 μM DNase I; (*lane 7*) 20 μM $t\beta_4$ + actin/DNase I complex (shown in *lane 6*); and (*lane 8*) 20 μM $t\beta_4$ + 6 μM DNase I.

complex of 43.8 ± 0.9 Å, a mean reduction of only 0.9 Å ($p = 0.018$).

Therefore, although the binding of $t\beta_4$ significantly decreases the FRET efficiency, the effect on the distance between these probes is not substantial. Fig. 3 *A* (*inset*) shows the emission spectrum of actin labeled with acceptor-only (*solid curve*), excited at 520 nm, and the same sample excited at 360 nm (*dashed curve*). From these data it is clear there can be no contribution of FITC fluorescence at 475 nm where the FRET is determined. DNase I binding does not alter the emission spectra of IAEDANS- or IAEDANS/FITC-actin (Fig. 3 *B*) nor does it affect the FRET efficiency between these sites (27). DNase I inhibits the $t\beta_4$-induced spectroscopic changes (Fig. 3) because it prevents $t\beta_4$ from binding to actin as assayed by native gel electrophoresis (Fig. 3 *D*), consistent with common or partially overlapping binding sites (8).

Effect of $t\beta_4$ on the distance between bound ε-ATP and Lys-61 of actin

FRET efficiencies between εATP and FITC were calculated from comparison of normalized fluorescence intensities of εATP/FITC- and εATP-actin in the absence and presence of $t\beta_4$. The distance between εATP and FITC attached to Lys-61 of actin (in the absence of $t\beta_4$ or DNase I) is 38.4 ± 0.8 Å, the R_0 is 47.4 Å, and the FRET efficiency is 0.78 ± 0.02 (17). Binding of $t\beta_4$ results in a 14 ± 3% ($n = 6$) increase in the εATP-actin fluorescence (Fig. 4), which is almost completely eliminated when $t\beta_4$ binds to εATP/FITC-actin, indicating that $t\beta_4$ binding increases the FRET efficiency between bound εATP and Lys-61. The precise value of the change in FRET efficiency was obtained by incubating samples with 0.4 mg/ml of trypsin in the presence of 2 mM ATP, which results in separation of the D- and A-probes and allows normalization of the reference fluorescence with respect to the εATP concentration (17). Unlabeled ATP readily competes with εATP bound to actin. The comparison of fluorescence intensities of digested ε-ATP/FITC- and εATP-actin is used for final normalization of FRET efficiency (see Methods). In the presence of $t\beta_4$, the normalized ratio of the fluorescence intensities of εATP/FITC-actin to that of εATP-actin is 0.16 ± 0.02, i.e., a FRET efficiency of 0.84 ± 0.02. Using an R_0 value of 48.1 Å (corrected for the $t\beta_4$-induced increased Q_D), the distance between the probes in the actin/$t\beta_4$ complex is 36.5 ± 1.0 Å. Thus, $t\beta_4$ closes the gap between the FITC probe on Lys-61 and εATP by 1.9 Å ($p < 0.000$).

Effect of $t\beta_4$ on the thermal stability of G-actin

Binding of $t\beta_4$ to G-actin results in thermal stabilization of actin monomers (Fig. 5). The thermal transition of actin monomers has a single maximum at 59.9°C, and an apparent calorimetric enthalpy (ΔH°_{app}) of 550 ± 20 kJ/mol ($n = 5$). $T\beta_4$ alone has no thermal transition (i.e., it is undistinguishable from the buffer baseline, data not shown), consistent with a disordered solution structure in the absence of actin (13). The thermal transition of actin in the presence of $t\beta_4$ occurs at 61.7°C, and the ΔH°_{app} increases to 620 ± 25 kJ/mol ($n = 5$). The width at the half-height of the thermal denaturation peak, $\Delta T_{0.5}$, is equal to 6.5°C for the actin/$t\beta_4$

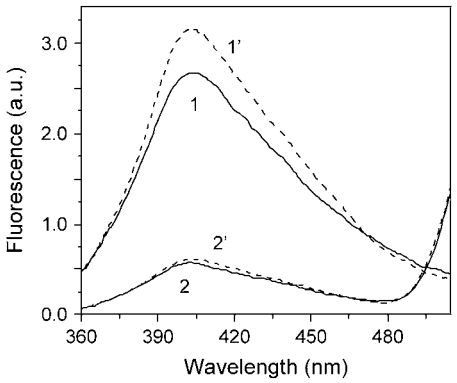

FIGURE 4 Effect of $t\beta_4$ on the distance between bound εATP and Lys-61 of actin. Corrected and averaged fluorescence spectra ($\lambda_{ex} = 315$ nm and $\lambda_{em} = 415$ nm) of εATP- and εATP/FITC-actin in the absence (*solid curves*) and presence of 10-fold molar excess $t\beta_4$ (*dashed curves*). The actin concentration was 1.5 μM in G-buffer containing 1 mM Tris/HCl pH 8.0 and 0.1 mM $CaCl_2$. The temperature was 10°C. Spectra were normalized to a labeling ratio of FITC to actin equal to one.

complex but it is 7.5°C for actin alone, suggesting a more cooperative thermal transition with $t\beta_4$ binding. The thermal denaturation of actin in the presence and absence of $t\beta_4$ was irreversible (data not shown). It is important to clarify that for calorimetric enthalpies of thermal transitions to be thermodynamically significant, denaturation must be reversible. Since actin denaturation is an irreversible process, the measured calorimetric enthalpies are best considered to be apparent thermodynamic parameters reflecting the nonequilibrium denaturation of actin (24).

Cofilin and $t\beta_4$ compete for binding to actin

Cofilin, $t\beta_4$, and their binary complexes with actin can be successfully resolved by native polyacrylamide gel electrophoresis (22,23), which has been employed previously to show an increased affinity of cofilin for actin in the presence

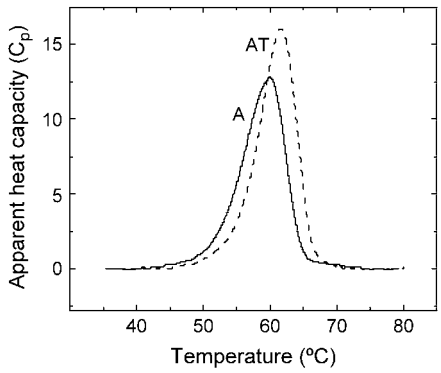

FIGURE 5 Effect of $t\beta_4$ on the thermal unfolding of actin. Representative DSC scans of G-actin (*A*) and actin-$t\beta_4$ (*AT*). The trace of $t\beta_4$ alone is not shown because it superimposes the buffer baseline. Conditions: 24 μM actin and 30 μM $t\beta_4$ in G-buffer. Heating rate is 1 K min^{-1}.

of DNase I (23). The actin/$t\beta_4$ complex migrates as a distinct band ahead of the actin monomers with free $t\beta_4$ appearing below the actin/$t\beta_4$ band (Fig. 6 *A*). Cofilin addition (molar ratios of $A/T/C = 1:5:2$) results in the appearance of a new band corresponding to the actin/cofilin complex. Excess cofilin ($A/T/C$ molar ratios of 1:5:7) competes and displaces $t\beta_4$ from the actin/$t\beta_4$ complex. Cofilin and $t\beta_4$ do not bind each other (*lane 1*, Fig. 6 *A*). The higher affinity of cofilin for actin monomers (1) accounts for the concentration-dependence of the competition. As expected for a reversible equilibrium reaction, cofilin and tβ_4 competitions are independent of the order of addition (Fig. 6 *B*). However, $t\beta_4$ does not compete with cofilin for actin binding in the presence of DNase I (Fig. 6 *C*), and the cofilin-DNase I-actin ternary complex (23) is stable even after the addition of a 15-fold molar excess $t\beta_4$ (Fig. 6 *C*). However, the addition of the same excess $t\beta_4$ to the actin/cofilin complex in the absence of DNase I leads to the dissociation of the actin/cofilin complex (Fig. 6 *D*). Importantly, under experimental conditions, binding of $t\beta_4$ to actin is completely abolished in the presence of DNase I, irrespective of the presence of cofilin (Fig. 3, *D* and *E*). We interpret these results to mean that accessibility to the DNase I binding loop is necessary for $t\beta_4$ to compete with cofilin for actin binding, presumably because SD2 forms part of the $t\beta_4$ binding site on actin and contributes to the high affinity.

DISCUSSION

This investigation was initiated to determine if $t\beta_4$ binding induces a conformational change in actin and to evaluate models of $t\beta_4$ binding to G-actin. $T\beta_4$ binding induces significant changes in the average conformation of actin monomers as measured by FRET. The distance between probes along one side of the monomer axis (Cys-374 to Gln-41) is increased, whereas the distance down the center (Cys-374 to Lys-61) decreases slightly. There is a significant reduction in the accessibility of the probe attached at Gln-41 when $t\beta_4$ binds, suggesting it forms part of the actin-$t\beta_4$ binding interface (5). The observation that $t\beta_4$ competes with cofilin and dissociates the cofilin-actin complex but not the cofilin-actin-DNase I ternary complex (Fig. 6) favors a role for SD2 in high affinity $t\beta_4$ binding. We conclude that $t\beta_4$ binds SD2 and rotates the DNase I-binding loop toward the nucleotide-binding site and away from SD1 (Fig. 1), providing a plausible structural mechanism for how $t\beta_4$ enhances the fluorescence of bound εATP (Fig. 4), changes the hydration (5), and reduces amide hydrogen exchange from actin (5). The nucleotide-dependence of SD2 conformation likely contributes to the nucleotide-dependence of the $t\beta_4$ binding affinity (5,28). When ATP bound to actin is exchanged for ADP, the DNase I binding loop adopts a folded α-helical conformation (11,12,29). $T\beta_4$ has a much higher affinity for ATP-actin than ADP-actin monomers (5,28), suggesting that the conformation of SD2 dictates how

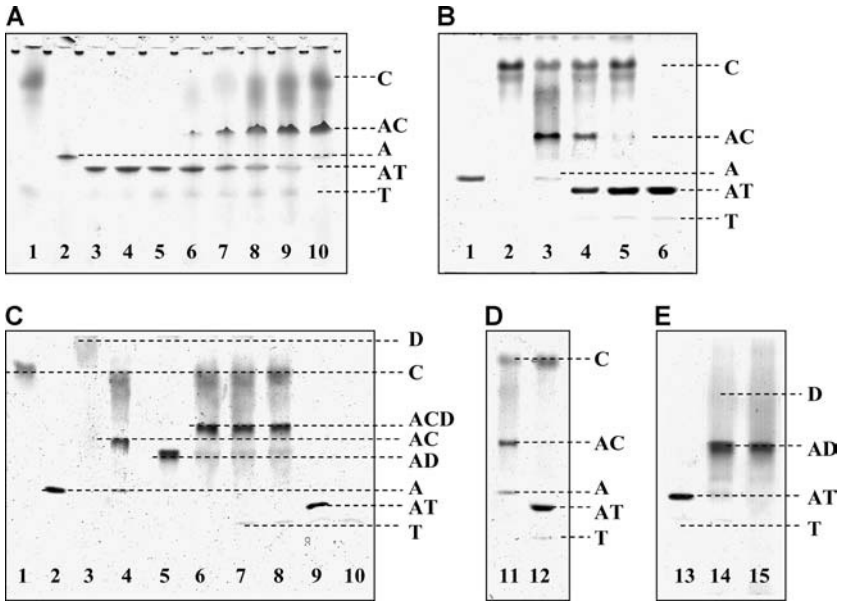

FIGURE 6 Effect of $t\beta_4$ on cofilin-actin and cofilin-actin-DNase I complexes. (*Panel A*) A representative 10% Native PAGE gel shows the effects of progressive addition of cofilin (*C*) to the preformed actin-$t\beta_4$ complex (*AT*). (*Lane 1*) A mixture of 14 μM *C* and 10 μM $t\beta_4$ (*T*); (*Lane 2*) 2 μM actin alone (*A*); (*Lanes 3–5*) a mixture of 2 μM *A* and 4, 6, and 10 μM *T*, respectively; (*Lanes 6–9*) titration of the preformed AT complex (2 μM *A* and 10 μM *T*) with 2, 6, 10, and 14 μM *C*, respectively; and (*Lane 10*) a mixture of 2 μM *A* and 14 μM *C*. (*Panel B*) A representative 10% Native PAGE gel shows the reverse order of ABP addition, i.e., progressive addition of *T* to the preformed *AC* complex. (*Lane 1*) *A* alone (3 μM); (*Lane 2*) *C* alone (9 μM); (*Lane 3*) a mixture of 3 μM *A* and 9 μM *C*; (*Lanes 4* and *5*) addition of 30 and 45 μM *T*, respectively, to the preformed *AC* complex (3 μM *A* and 9 μM *C*); and (*Lane 6*) a mixture of 3 μM *A* and 45 μM *T*. (*Panel C*) A representative 10% Native PAGE gel shows *C* (12 μM), *A* (3 μM), DNase I (*D*, 5 μM), and *T* (45 μM) alone (*lanes 1*, *2*, *3*, and *10*, respectively). The binary complexes of *A* with *C*, *D*, and *T* are shown (*lanes 4*, *5*, and *9*, respectively). (*Lane 6*) The ternary complex formed by *A*, *C*, and *D* (*A*/*C*/*D* = 1:1.6:4) in the absence of *T*. (*Lane 7*) The addition of a 15-fold molar excess *T* to the preformed ternary *ACD* complex (shown in *lane 6*). (*Lane 8*) The addition of *D* to preformed *AT* (1:15) complex in the presence of a fourfold unbound *C* (this sample before addition of *D* is shown in *lane 12*, Gel *D*). (*Panel D*) A representative 10% Native PAGE gel shows the *AC* (1:4) complex (*lane 11*), and the addition of a 15-fold molar excess *T* to it (*lane 12*). (*Panel E*) This 10% Native PAGE gel shows the *AT* (1:15) complex (*lane 13*); the addition of a 1.6-fold molar excess *D* to it (*lane 14*); and the control *AD* (1:1.6) binary complex (*lane 15*). Gels were run simultaneously.

tightly $t\beta_4$ binds actin (12) and that the higher affinity of $t\beta_4$ for ATP-actin results from stabilizing contacts made with SD2 (5,8).

The detailed three-dimensional structure of the actin-$t\beta_4$ complex has not been determined experimentally. However, two alternatives have been proposed for $t\beta_4$ binding to actin monomers, based on structures of actin bound to $t\beta_4$ homologs (6,7). Hertzog et al. (6) reported the structure of actin bound to domain 1 of ciboulot, which shares 30% sequence identity with tβ_4, while Irobi et al. (7) reported the structure of actin bound to a construct consisting of tβ_4 residues 21–43 fused to the C-terminus of gelsolin segment 1 (gelsolin residues 27–152). Both Hertzog's and Irobi's structures indicate that the N-terminal helix of tβ_4 binds SD1 and SD3 of actin, and show the central region of tβ_4 (residues 15–29) in an extended conformation overlying the nucleotide binding cleft. In both models, the C-terminus of tβ_4 contacts the pointed end of the actin monomer, although the two models differ in the site of contact. Hertzog et al. (6) favor the C-terminus of $t\beta_4$ binding directly to SD2 as we proposed (5,8), while Irobi et al. (7) showed residues 30–40 of $t\beta_4$ in an α-helix positioned between actin SD2 and SD4 on the pointed end; the three C-terminal residues of $t\beta_4$ are unresolved in this structure. This is consistent with our crosslinking studies (5,8), which showed that the N-terminus of $t\beta_4$ contacts the barbed end of actin, while its C-terminus contacts the pointed end. However, some features of the crystallographic structures, and the models for actin-$t\beta_4$ based on them, are likely to differ from the actual structure of actin-$t\beta_4$.

Ciboulot and $t\beta_4$ have opposite effects on actin tryptophan fluorescence and on the fluorescence of AEDANS-labeled actin. In addition, while $t\beta_4$ acts as a pure sequestering protein, ciboulot promotes monomer addition to barbed ends (31). Ciboulot and $t\beta_4$ show substantial sequence homology. However, nonhomologous substitutions occur at several residues, which have been shown by NMR to form close contacts with actin (13). In particular, polar residues T20 and N26 in $t\beta_4$ are replaced by hydrophobic residues in ciboulot, and Domanski et al. (13) suggest that these substitutions result in differences between the binding sites of the C-terminal segments of ciboulot and $t\beta_4$. Such differences in the binding of the C-terminal segment may contribute to the observed differences in activity. The design of the gelsolin-$t\beta_4$ construct was similarly based on limited sequence homology, in this case between $t\beta_4$ residues 17–23 (LKKTETQ) and gelsolin residues 149–155 (FKHVVPN) (7). Considering that gelsolin segment 1 binds actin with ~100-fold higher affinity than even full-length $t\beta_4$ (32), the gelsolin domain must provide most of the binding energy for the gelsolin-$t\beta_4$ construct. Thus the position of the gelsolin binding site on actin may constrain the binding of the $t\beta_4$ segment of the construct, so as to favor a binding mode that is less favorable for full-length $t\beta_4$.

The conformation of actin SD2 and its contact with $t\beta_4$ in the complex remain to be determined, since it was not fully resolved in either structure. Our results, particularly the reduced solvent exposure of Gln-41, strongly favor direct interaction of $t\beta_4$ with SD2 of actin, and therefore support

this feature of the Hertzog structure, in contrast to that of Irobi et al. The fact that limited proteolysis of actin on SD2 did not affect the binding of $t\beta_4$ in an earlier study (13), rather than indicating a lack of contact, may indicate that $t\beta_4$ binding favors a protease-susceptible conformation of SD2 consistent with conformational rearrangement of this region of actin. The position of $t\beta_4$ residues 30–40, which Irobi et al. (7) observe in their crystal structure, may be influenced by several factors. Our original NMR and CD study of the actin-$t\beta_4$ complex (8) showed that although $t\beta_4$ becomes more structured when bound to actin, it retains substantial segmental mobility. The high mobility in the bound state suggests that $t\beta_4$ may bind actin in multiple modes with comparable energies that exist in dynamic equilibrium as demonstrated for tropomyosin and actin filaments (30,33). The equilibrium between these modes would likely be dependent on experimental conditions, and thus be influenced by crystal packing forces, ionic composition, and osmolarity of the crystallization solvent. In addition, the structure of the gelsolin-$t\beta_4$ fusion protein and the position of the gelsolin binding site on actin may favor a binding mode that is less favorable for full-length $t\beta_4$. A dynamic $t\beta_4$ C-terminus could account for the apparently conflicting biochemical solution studies demonstrating that $t\beta_4$ can be chemically crosslinked to SDs 1, 2, and 3 (5,8) as well as the actin-bound nucleotide (34).

The principal biological effect of $t\beta_4$ is to maintain a reservoir of unpolymerized ATP-actin monomers. Spontaneous polymerization is inhibited by blocking sites involved in intersubunit interactions (22). The FRET data indicate that stable binding to ATP-actin monomers is coupled to reorganization of actin SD2, which is likely to account for the specificity for ATP-actin over ADP-actin monomers. In this respect $t\beta_4$ differs from cofilin, which also inhibits nucleotide exchange but binds preferably to ADP-actin monomers (1). In addition, the competition between cofilin and $t\beta_4$ for binding actin may contribute to the balance between F- and G-actin in living cells by modulating dynamics of filament assembly/disassembly at the barbed and pointed ends (1). The ability to modulate the conformation of SD2 may account for the different affinities of $t\beta_4$ for ATP- and ADP-actin, and allows $t\beta_4$ to maintain a large reservoir of unpolymerized ATP-actin monomers.

We thank Dr. D. I. Levitsky (Bach Research Institute, Moscow, Russia) and Dr. D. Chhabra (University of Sydney) for advice.

I.V.D. was supported by grants from the Australian Research Council and the National Health and Medical Research Council of Australia, The Young Australian Researcher 2000 Award from The Australian Academy of Science, and The James Kentley Memorial Scholarship from the University of Sydney, Australia. E.M.D.L.C. was supported by a Hellman Family Fellowship and grants from the American Heart Association (No. 0235203N) and the National Science Foundation (No. MCB-0216834).

REFERENCES

1. dos Remedios, C. G., D. Chhabra, M. Kekic, I. V. Dedova, M. Tsubakihara, D. A. Berry, and N. J. Nosworthy. 2003. Actin binding proteins: regulation of cytoskeletal microfilaments. *Physiol. Rev.* 83: 433–473.
2. Devineni, N., L. S. Minamide, M. Niu, D. Safer, R. Verma, J. R. Bamburg, and V. T. Nachmias. 1999. A quantitative analysis of G-actin binding proteins and the G-actin pool in developing chick brain. *Brain Res.* 823:129–140.
3. Goldschmidt-Clermont, P. J., M. I. Furman, D. Wachsstock, D. Safer, V. T. Nachmias, and T. D. Pollard. 1992. The control of actin nucleotide exchange by thymosin β4 and profilin. A potential regulatory mechanism for actin polymerization in cells. *Mol. Biol. Cell.* 3:1015–1024.
4. Ballweber, E., E. Hannappel, T. Huff, H. Stephan, M. Haener, N. Taschner, D. Stoffler, U. Aebi, and H. G. Mannherz. 2002. Polymerization of chemically cross-linked actin·thymosin β4 complex to filamentous actin: alteration in helical parameters and visualization of thymosin β4 binding on F-actin. *J. Mol. Biol.* 315:613–625.
5. De La Cruz, E. M., E. M. Ostap, R. A. Brundage, K. S. Reddy, H. L. Sweeney, and D. Safer. 2000. Thymosin-β4 changes the conformation and dynamics of actin monomers. *Biophys. J.* 78:2516–2527.
6. Hertzog, M., C. van Heijenoort, D. Didry, M. Gaudier, J. Coutant, B. Gigant, G. Didelot, T. Preat, M. Knossow, E. Guittet, and M. F. Carlier. 2004. The β-thymosin/WH2 domain; structural basis for the switch from inhibition to promotion of actin assembly. *Cell.* 117: 611–623.
7. Irobi, E., A. H. Aguda, M. Larsson, C. Guerin, H. L. Yin, L. D. Burtnick, L. Blanchoin, and R. C. Robinson. 2004. Structural basis of actin sequestration by thymosin-β4: implications for WH2 proteins. *EMBO J.* 23:3599–3608.
8. Safer, D., T. R. Sosnick, and M. Elzinga. 1997. Thymosin β4 binds actin in an extended conformation and contacts both the barbed and pointed ends. *Biochemistry.* 36:5806–5816.
9. Ballweber, E., K. Giehl, E. Hannappel, T. Huff, B. M. Jockusch, and H. G. Mannherz. 1998. Plant profilin induces actin polymerization from actin: β-thymosin complexes and competes directly with β-thymosins and with negative co-operativity with DNase I for binding to actin. *FEBS Lett.* 425:251–255.
10. Tirion, M. M., and D. ben-Avraham. 1993. Normal mode analysis of G-actin. *J. Mol. Biol.* 230:186–195.
11. Otterbein, L. R., P. Graceffa, and R. Dominguez. 2001. The crystal structure of uncomplexed actin in the ADP state. *Science.* 293: 708–711.
12. De La Cruz, E. M., and T. D. Pollard. 2001. Structural biology. Actin' up. *Science.* 293:616–618.
13. Domanski, M., M. Hertzog, J. Coutant, I. Gutsche-Perelroizen, F. Bontems, M. F. Carlier, E. Guittet, and C. van Heijenoort. 2004. Coupling of folding and binding of thymosin β4 upon interaction with monomeric actin monitored by nuclear magnetic resonance. *J. Biol. Chem.* 279:23637–23645.
14. Dedova, I. V., V. N. Dedov, N. J. Nosworthy, B. D. Hambly, and C. G. dos Remedios. 2002. Cofilin and DNase I affect the conformation of the small domain of actin. *Biophys. J.* 82:3134–3143.
15. Tao, T., and J. Cho. 1979. Fluorescence lifetime quenching studies on the accessibilities of actin sulfhydryl sites. *Biochemistry.* 18:2759–2765.
16. Burtnick, L. D. 1984. Modification of actin with fluorescein isothiocyanate. *Biochim. Biophys. Acta.* 791:57–62.
17. Miki, M., C. G. dos Remedios, and J. A. Barden. 1987. Spatial relationship between the nucleotide-binding site, Lys-61 and Cys-374 in actin and a conformational change induced by myosin subfragment-1 binding. *Eur. J. Biochem.* 168:339–345.
18. Bernhardt, R., N. T. Ngoc Dao, H. Stiel, W. Schwarze, J. Friedrich, G. R. Janig, and K. Ruckpaul. 1983. Modification of cytochrome P-450 with fluorescein isothiocyanate. *Biochim. Biophys. Acta.* 745: 140–148.
19. De La Cruz, E. M., and T. D. Pollard. 1995. Nucleotide-free actin: stabilization by sucrose and nucleotide binding kinetics. *Biochemistry.* 34:5452–5461.

20. Nyitrai, M., G. Hild, Z. Lakos, and B. Somogyi. 1998. Effect of Ca^{2+}-Mg^{2+} exchange on the flexibility and/or conformation of the small domain in monomeric actin. *Biophys. J.* 74:2474–2481.

21. Van Der Meer, B. W. 1994. The donor quantum yield. *In* Resonance Energy Transfer. B.W. Van Der Meer, G. Coker, and S.-Y. Chen, editors. VCH Publishers, New York. 20–23.

22. Safer, D., R. Golla, and V. T. Nachmias. 1990. Isolation of a 5-kiloDalton actin-sequestering peptide from human blood platelets. *Proc. Natl. Acad. Sci. USA.* 87:2536–2540.

23. Kekic, M., N. J. Nosworthy, I. Dedova, C. A. Collyer, and C. G. dos Remedios. 2001. Regulation of the cytoskeleton assembly: a role for a ternary complex of actin with two actin-binding proteins. *In* Molecular Interactions of Actin. Actin Structure and Actin-Binding Proteins. C.G. dos Remedios and D.D. Thomas, editors. Springer-Verlag, Berlin. 165–181.

24. Nikolaeva, O. P., I. V. Dedova, I. S. Khvorova, and D. I. Levitsky. 1994. Interaction of F-actin with phosphate analogues studied by differential scanning calorimetry. *FEBS Lett.* 351:15–18.

25. Kim, E., and E. Reisler. 1996. Intermolecular coupling between loop 38–52 and the C-terminus in actin filaments. *Biophys. J.* 71:1914–1919.

26. Kabsch, W., H. G. Mannherz, D. Suck, E. F. Pai, and K. C. Holmes. 1990. Atomic structure of the actin·DNase I complex. *Nature.* 347:37–44.

27. dos Remedios, C. G., P. C. Kiessling, and B. D. Hambly. 1994. DNase I binding induces a conformational change in the actin monomer. *In* Synchrotron Radiation in the Bioscience. B. Chance, editor. Oxford University Press, New York. 418–425.

28. Carlier, M. F., C. Jean, K. J. Rieger, M. Lenfant, and D. Pantaloni. 1993. Modulation of the interaction between G-actin and thymosin β4 by the ATP/ADP ratio: possible implication in the regulation of actin dynamics. *Proc. Natl. Acad. Sci. USA.* 90:5034–5038.

29. Graceffa, P., and R. Dominguez. 2003. Crystal structure of monomeric actin in the ATP state. Structural basis of nucleotide-dependent actin dynamics. *J. Biol. Chem.* 278:34172–34180.

30. Xu, C., R. Craig, L. Tobacman, R. Horowitz, and W. Lehman. 1999. Tropomyosin positions in regulated thin filaments revealed by cryo-electron microscopy. *Biophys. J.* 77:985–992.

31. Hertzog, M., E. G. Yarmola, D. Didry, M. R. Bubb, and M.-F. Carlier. 2002. Control of actin dynamics by proteins made of β-thymosin repeats. *J. Biol. Chem.* 277:14786–14792.

32. Bryan, J. 1988. Gelsolin has three actin-binding sites. *J. Cell Biol.* 106:1553–1562.

33. Bacchiocchi, C., and S. S. Lehrer. 2002. Ca^{2+}-induced movement of tropomyosin in skeletal muscle thin filaments observed by multi-site FRET. *Biophys. J.* 82:1524–1536.

34. Reichert, A., D. Heintz, H. Echner, W. Voelter, and H. Faulstich. 1996. Identification of contact sites in the actin-thymosin β4 complex by distance-dependent thiol cross-linking. *J. Biol. Chem.* 271:1301–1308.